Land-use changes in Amazon and Atlantic rainforests modify organic matter and black carbon compositions transported from land to the coastal ocean

Tassiana Soares Gonçalves Serafim, Marcelo Gomes de Almeida, Gérard Thouzeau, Emma Michaud, Jutta Niggemann, Thorsten Dittmar, Michael Seidel, Carlos Eduardo de Rezende

Land-use changes in Amazon and Atlantic Rainforests modify organic matter and black carbon compositions transported from land to the coastal ocean

Tassiana Soares Gonçalves Serafim[a,*], Marcelo G. Almeida[b], Gérard Thouzeau[c], Emma Michaud[c], Jutta Niggemann[d], Thorsten Dittmar[d,e], Michael Seidel[d], Carlos E. Rezende[b]

[a] Leibniz Institute for Baltic Sea Research Warnemünde, Seestrasse 15, 18119 Rostock, Germany

[b] Laboratório de Ciências Ambientais, Centro de Biociências e Biotecnologia, Universidade Estadual do Norte Fluminense Darcy Ribeiro, Campos dos Goytacazes RJ, CEP 28013-602, Brazil

[c] Univ Brest, CNRS, IRD, Ifremer, UMR 6539 - LEMAR, F-29280 Plouzané, France

[d] Research Group for Marine Geochemistry (ICBM-MPI Bridging Group), Institute for Chemistry and Biology of the Marine Environment, Carl von Ossietzky University Oldenburg, Germany

[e] Helmholtz Institute for Functional Marine Biodiversity (HIFMB) at the University of Oldenburg, Germany

* Corresponding author: Serafim, T.S.G., e-mail: tassiana.sgs@gmail.com

Abstract: This study assessed black carbon (BC) dynamics, concentrations, and the organic matter (OM) isotopic carbon composition in northeastern South America drainage basin coastal sediments. Paraíba do Sul (PSR; Atlantic Rainforest, Brazil) coastal sediments displayed more ^{13}C-enriched values (-22.6 ± 1.3 ‰ [*n* = 13]) than Amazon and Sinnamary (Amazon Rainforest in French Guiana and Brazil) sediments (-25.0 ± 3.1 ‰ [*n* = 14] and -26.1 ± 1.0 ‰ [*n* = 6], respectively), indicating that local land-use basin changes have altered the OM composition, *i.e.*, from natural C_3 plant to C_4 plants contributions. BC contents normalized to total organic carbon (TOC) content were 0.32 ± 0.24 (*n* = 8), 0.73 ± 0.67 (*n* = 6), and 0.95 ± 0.74 (*n* = 13) mg g^{-1} TOC for Amazon, Sinnamary and PSR samples, respectively, with BC sources appearing to differ according to different drainage basin vegetation covers. With increasing distance from the river mouths, BC contents exhibited different trends between the coastal zones, with values increasing for the PSR and decreasing values for the Amazon samples. BC distribution in Sinnamary coastal sediments did not display specific patterns. Regarding the Amazon coastal zone, BC contents decreased while the B6CA:B5CA ratios did not show a pattern, which could indicate that BC in the area originates from river transport (aged BC) and that the hydrophobic component of dissolved BC is removed. The BC content mostly increased in the PSR coastal zone, while the B6CA:B5CA ratios were not altered for the entire gradient, indicating the BC stability and possible atmospheric deposition of soot. Our findings indicate that different sources, transformation processes, and hydrological conditions affect BC contents within coastal zones. Continuous land cover changes in both the Amazon and Atlantic Rainforests may result in large-scale marine carbon cycling impacts.

51 Keywords: Black carbon; Amazon Rainforest; Atlantic Rainforest; Carbon
52 isotopic composition; Coastal sediments; Organic matter.

1. INTRODUCTION

The conversions of primary forest areas to croplands and agricultural areas have devastated the Brazilian Atlantic Rainforest, destroying important biomes such as the world's largest forest, the Amazon Rainforest (Ferrante and Fearnside, 2019), modifying organic matter (OM) soil contents (Bernardes et al., 2004). Native forest vegetation conversion has altered the Atlantic Rainforest landscape, with about 28 % of the original vegetation cover now distributed only in fragments (Rezende et al., 2018; Solórzano et al., 2021). Such anthropogenic areas currently comprise approximately 15 % of the entire Amazon biome (Stahl et al., 2016), and are now on the rise due to the destruction of forest areas. One strategy applied to forest biomass removal and the management of anthropogenic regions consists in fire cleaning (Edwards, 1984). Fire is currently considered the primary Amazon Rainforest biomass removal vector, through forest fires caused by drought events (Aragão et al., 2018) or anthropogenic activities, such as cattle pasture expansion and management and agricultural activities. Wildfires and anthropogenic burning globally emit about 2.2 Pg of carbon per year in the form of greenhouse gases (Werf et al., 2017). Furthermore, fires also produce another carbon-enriched form displaying higher resistance to degradation than non-thermally-altered OM, named black carbon (BC) (Forbes et al., 2006; Bird and Ascough, 2012).

Black carbon is commonly described as the thermally altered and condensed aromatic OM fraction produced after incomplete combustion of plant biomasses or fossil fuels (Goldberg, 1985). Hedges et al. (2000) described the broad spectrum of BC compounds as a combustion continuum, later termed the degradation continuum (Bird et al., 2015), ranging from levoglucosan to highly

condensed aromatic compounds that may display environmental persistence (Wagner et al., 2021). The global production of BC derived from plant biomasses has been estimated as ranging between 50 and 300 Tg of BC per year (Forbes et al., 2006; Bird et al., 2015) and about 80 % of BC initially remains in BC production sites following combustion (Kuhlbusch and Crutzen, 1995). According to Reisser et al. (2016), BC comprises about 14 % of overall soil OM, with an average residence time of 88 years. This residence time, however, can range from a few years to millennia, depending on the combination of physical, chemical, and microbial processes (Singh et al., 2012). Black carbon mobilization from soils and its entry into aquatic systems occurs mainly through the dissolved phase following solubilization of historical BC (Dittmar, 2008; Dittmar et al., 2012b) and lateral particle transport, mainly due to soil erosion (Major et al., 2010). In addition, BC inputs into aquatic systems can take place, to a smaller extent, via atmospheric transport, and its deposition can take place along the entire continent-ocean gradient (Jurado et al., 2008; Coppola et al., 2018).

Increased erosion due to land-use conversion increases particle transport into the aquatic system, resulting in the global accumulation of 75 Tg sediments per year, mainly in areas below 2000 m altitude (Wilkinson & McElroy, 2007). These eroded particles travel throughout the water column and eventually become deposited along the continent-ocean gradient, mainly in continental areas and transition zones, with only about 20 % of this suspended particulate matter (SPM) reaching their destination, the marine sediments (Bird et al., 2015; Coppola et al., 2018). The transport of SPM and associated OM along the continent gradient is influenced by river and drainage basin

characteristics (Burdige, 2007). Suspended particulate matter transport is faster in small rivers usually associated with mountains, narrow continental shelves, or active continental margins, resulting in relatively low OM remineralization rates along the continent-ocean gradient (Blair et al., 2003). In contrast, SPM is subject to deposition and resuspension cycles in large rivers, resulting in increased OM remineralization due to long residence times (Aller, 1998). Additionally, OM (and BC) transported alongside particles can be replaced downstream by OM produced at lower elevations (Aller et al., 1996; Burdige, 2007).

By estimating BC contents associated with SPM and sediments of both large (e.g., the Amazon, Congo) and small (e.g., the Eel, Santa Clara, Danube) rivers, Coppola et al. (2018) reported that BC comprised about 15.8 ± 0.9 % of total organic carbon (TOC) content, and the data did not indicate associations between BC contents and river size. Furthermore, BC export dynamics in the rivers were attributed to soil erosion, where BC generally undergoes constant pre-ageing despite environmental conditions and settings. However, SPM transport to the ocean is considerably reduced due to strong physicochemical gradients, favoring certain processes, such as flocculation, in estuarine zones (Eisma, 1986). Regnier et al. (2013) estimated that about 20 % of the TOC associated with SPM does not reach the open ocean, due to deposition along continent–coastal gradients. The global flux of particulate BC to the ocean ranges from 19 to 80 Tg per year (Bird et al., 2015), assuming that BC comprises between 5 and 15 % of the TOC content (Cole et al., 2007). Lohmann et al. (2009) reported that BC accounted for between 3 and 35 % of OC contents in deep-sea sediments from the South Atlantic Ocean. These

128 authors estimated the most recalcitrant form obtained by the degradation
129 continuum model by isolating soot BC through the thermochemical oxidation
130 technique and attributing its primary source as terrestrial by analyzing the
131 isotopic organic carbon ($\delta^{13}C$) composition. To evaluate environmental BC
132 sources, $\delta^{13}C$ values are often associated with BC content, as reported by Liu
133 and Han (2021), who coupled BC content with $\delta^{13}C$ results and reported that
134 the main source of BC associated to SPM in the Xijiang River Basin, in
135 Southeast China, is fossil fuel combustion, accounting for around 80 % of the
136 total BC content.

137 In this context, BC spatial dynamics and concentrations were assessed
138 in the coastal sediments of three northeastern South American drainage basins.
139 The Sinnamary (French Guiana) and Amazon River (Brazil) basins are covered
140 by primary forest vegetation (terrestrial C_3 plants), whereas the Paraíba do Sul
141 River (PSR; Brazil) basin is mainly covered with grasses (terrestrial C_4 plants),
142 due to land-use changes. We further evaluated if the transition from primary
143 forests to pasture and cultivation areas has altered the sources and composition
144 of the OM deposited in associated coastal sediments. Black carbon content was
145 analyzed by the benzene-polycarboxylic acid (BPCA) method, and elemental
146 and isotopic OM compositions of bulk total organic carbon (TOC and $\delta^{13}C$), as
147 well as nitrogen (N and $\delta^{15}N$) were determined. Three hypotheses were tested:
148 (1) the OM of the PSR is ^{13}C-enriched compared to the Amazon River, due to
149 vegetation basin cover alterations; (2) the BC content in the Amazon River
150 coastal zone is lower compared to the other evaluated coastal sediments as a
151 result of OM dilution and floodplain replacement; and (3) BC content is directly
152 related to land use alterations in the PSR coastal zone and not to historical

153 Atlantic Rainforest burning, as suggested previously for dissolved BC (Dittmar
154 et al., 2012; Marques et al. 2017).

155 ## 2. MATERIAL AND METHODS

156 ### 2.1. Study areas

157 #### 2.1.1. The Amazon and French Guiana coastal zones

158 The Amazon Rainforest extends over several countries, including Brazil
159 and French Guiana. Its surface area represents about 45 % of the world's
160 remaining tropical forests (Laurance et al., 2001), which comprises
161 approximately 4 % of the Earth's surface (about 6,100,000 km^2) (Malhi et al.,
162 2008; Gallo and Vinzon, 2015). The Amazon Rainforest, besides playing an
163 essential role in storing carbon in its biomass, is responsible for transporting
164 terrestrial carbon to the Atlantic Ocean via the Amazon River (Cai et al.,1988;
165 Malhi et al., 2006, 2008). The Amazon River exhibits a seasonal cycle with
166 maximum discharge reaching an average of 209,000 m^3 s^{-1} from May to July
167 (Latrubesse, 2008). Material discharges to the coastal zone comprise
168 approximately 20 % of the global input of terrestrial material to the ocean
169 (Richey et al., 1986; Ward et al., 2015). Due to the basin’s climate, strong
170 erosion and rapid particle deposition processes can lead to rapid sedimentation
171 rate changes in the Amazon River plume area (Kuehl et al., 1986). The plume
172 moves in a northwestern direction, and it has been suggested that a large
173 portion of the OM in the sedimentary compartment of the Brazilian shelf and
174 adjacent northwestern areas originates from the Amazon basin (Wells and
175 Coleman, 1981; Nittrouer et al., 1986). Approximately 20 % of the SPM
176 reaching the coastal zone is carried towards French Guiana, due to interactions

between the Brazilian North Current, east trade winds, and semi-diurnal sea currents (Geyer et al., 1996; Aller et al., 2004).

French Guiana vegetation cover comprises 97 % of tropical forest (Chave et al., 2001), with extensive mangrove forests covering over 80 % of the coast (Fromard et al., 2004). The Sinnamary River is considered a small river, and its drainage basin extends over 6,565 km^2, with seasonal river discharges (Richard et al., 2000; Ray et al., 2018). The minimum and maximum discharge averages range between 193 and 700 m^3 s^{-1} in November (dry season) and June (wet season) 2015, respectively (Ray et al., 2018; source: DEAL GUYANE-EDF). According to Oliveira and Clavier (2000) and Merona (2005), water discharge variations in this area depends on the anthropogenic process of opening an upstream dam and the natural El Niño event. The Sinnamary River estuary undergoes a macro tidal regime, with a tidal range of ca. 3 m near the river mouth (Ray et al., 2018). The estuary's extensive mangrove forests are dominated by *Avicennia germinans* (Marchand et al., 2003, Marchand, 2017).

2.1.2. The Paraíba do Sul coastal zone

The Paraíba do Sul River (PSR) basin, comprising 57,000 km^2, extends over the states of São Paulo, Rio de Janeiro, and Minas Gerais in southeastern Brazil (Ovalle et al., 2013). The PSR occupies an area previously entirely covered by Atlantic Rainforest, and about 74 % of its basin is currently covered by pasture and sugar-cane crop areas (Figueiredo et al., 2011; Marques et al., 2017). Due to these changes, the basin has suffered from intense erosion, leading to higher particle inputs to the local aquatic system. The PSR estuary and the second largest mangrove forest in the state of Rio de Janeiro are located in São João da Barra, in the Norte Fluminense region (Bernini and

202 Rezende, 2004). The PSR is a small- to a medium-sized river, whose
203 discharges depend on the season. In the dry period, between June and
204 September, PSR discharge rates vary between 200 and 500 $m^3 s^{-1}$, reaching a
205 maximum of 2,600 $m^3 s^{-1}$ during the rainy period (Silva et al., 2001). The wet
206 season of 2014 was atypical, due to low precipitation rates caused by sea level
207 pressure anomalies in Southeastern Brazil, influenced by the La Niña event,
208 causing extreme rain events.

209 **2.2. Sampling**

210 Surface sediment samples (0 - 2 cm) were obtained employing different
211 techniques, totaling 33 samples distributed into six (hand core sampling), 14
212 (multicore sampler), and 13 (boxcore sampler) samples from the coastal
213 Sinnamary River (5°21' - 5°30'N and 52°56' - 53°3'W), the Amazon River (2°S -
214 4°N and 46° - 51°W), and the PSR (21°28' - 21°40'S and 40°48' - 41°6'W) area,
215 respectively (Figure 1; Supplementary Table 1). Samples from the Sinnamary
216 and PSR coastal zones were obtained near mangroves located in the intertidal
217 estuarine zones, while Amazon samples were collected in the subtidal area
218 under the influence of the Amazon plume. The sample sets were obtained
219 during the wet season in January 2019, April 2018, and February 2014 at the
220 Sinnamary, Amazon, and PSR coastal zones, respectively. The sediments were
221 immediately frozen (-20 °C) after sampling until further analyses.

222

223 **Figure 1.** South America sediment sampling sites: (A) the Sinnamary estuary,
224 in the French Guiana (B), the Paraíba do Sul River estuary, in southeastern
225 Brazil (C) and the Amazon plume, in northern Brazil (D).

226

2.3. Elemental and isotopic organic matter compositions

Sediment samples were freeze-dried in the laboratory and homogenized. For the TOC and $\delta^{13}C$ determinations, samples (10 mg) were acidified in silver capsules for carbonate removal using 2M HCl. For the N and $\delta^{15}N$ determinations, samples (10 mg) were weighed into tin capsules. Elemental and isotopic values were obtained using a Flash 2000 elemental analyzer coupled to a Delta V mass spectrometer, with an uncertainty of measurement of 0.05 % for OC, 0.03 % for N, and ± 0.2 ‰ for $\delta^{15}N$ and $\delta^{13}C$.

2.4. Black carbon determination

Black carbon contents were determined according to Glaser et al. (1998) and Brodowski et al. (2005) with slight adaptations. The samples were pre-digested with 10 mL trifluoroacetic acid for 4 h in a high-pressure system at 100 ± 5 °C, followed by filtering through GF/F filters (Whatman, pore size 0.7 µm). The filters were then placed in an oven for 2 h at 40 °C. After drying, 2 mL of nitric acid were added, and the samples were digested at 165 ± 5 °C for 8 h to obtain BPCAs from OM oxidation. The samples were again filtered through cellulose acetate filters (pore size 0.2 µm), and 8 mL of ultrapure water were added to dilute the applied nitric acid. A total of 50 µL of a surrogate (phthalic acid, 1 mg mL^{-1}) were added to 2.5 mL sample aliquots to correct for losses during the cleaning procedure, where the recovery was 60 ± 17 %, indicating sample losses during the process. Sample purification was conducted employing columns containing cation exchange resins after conditioning (Dowex 50 WX 8, 200-400 mesh, Fluka, Steinheim, Germany). The obtained sample volumes were separated into four vials and freeze-dried, resuspended with methanol and, finally, dried with N_2. The last sample cleaning step

252 consisted in adding 4 mL of pyridine, a centrifugation step, and a new drying
253 step with N_2. The samples were then analyzed by gas chromatography (GC-MS)
254 and ultra-performance liquid chromatography (UPLC), according to Stubbins et al.
255 (2015). The samples were derivatized for the GC-MS analysis using 250 µL of
256 pyridine and 250 µL of *N*,*O*-bis (trimethylsilyl) trifluoroacetamide with 1 %
257 trimethylchlorosilane (BSTFA-TMCS, 99:1) followed by heating for 2 h at 80 °C
258 and then injected into the GC-MS. Biphenyl-2,2'-dicarboxylic acid was added as
259 the internal standard before sample derivatization as an internal calibration of
260 the GC-MS. Concerning the UPLC analysis, samples were dried with N_2 and
261 resuspended in a phosphate buffer 100 µL (Na_2HPO_4 and NaH_2PO_4 each 5 mM
262 in ultrapure water, pH 7.2).
263 The correction factor of 1.5 suggested by Schneider et al. (2011) was
264 used for the samples analyzed via GC-MS to compare the data obtained by the
265 different approaches since Schneider et al. (2011) reported analytical variability
266 when comparing gas and liquid chromatography analyses. Other conversion
267 factors reported for the BPCA method (i.e., Glaser et al., 1998) were not
268 applied, as also suggested by Schneider et al. (2011). The standard reference
269 sediment NIST 1941b was used to accurately and precisely determine BPCA
270 contents. The mean BC content, normalized by the TOC content, detected by
271 the GC-MS was 2.08 ± 0.17 mg g^{-1} TOC (n = 5), and the UPLC value was 2.97
272 ± 0.26 mg g^{-1} TOC (n = 3). The other two digestion products, B3CA and B4CA,
273 were not assessed, as Kappenberg et al. (2016) demonstrated that these
274 groups may be produced after the oxidation of non-pyrogenic OM, even when
275 employing low sample weights (< 5 mg TOC). However, to allow for further
276 comparisons, we also considered B3CA and B4CA with the conversion factor

277 2.27 from Glaser et al. (1998). Accordingly, the BC/TOC ratios and the BC
278 contribution for the dry weight sediment found for NIST 1941b were 1.97 ± 0.48
279 and 0.05 ± 0.30 %, respectively, comparable to previously reported values by
280 Hammes et al. (2007), with BC accounting for 0.06 ± 0.01 % of the dry sediment
281 weight and BC/TOC ratios between 2.0 and 8.6.

282 **2.5. Organic matter sources**

283 Bayesian mixing models provide a synthesis of source and mixture data
284 within a model structure that incorporates data variability (e.g., isotopic
285 fractionation factor) (Parnell et al., 2010; Stock and Semmens, 2016), while
286 linear mixing models consider that diagenetic changes do not significantly alter
287 $\delta^{13}C$ and $\delta^{15}N$ OM values. Thus, the Bayesian MixSIAR mixing model was used
288 to estimate the source contributions of each sample (Stock and Semmens,
289 2016; Stock et al., 2018). The MixSIAR applied Bayesian isotopic mixing and
290 fitting models employing Markov chain Monte Carlo (MCMC) simulations of
291 plausible values consistent with the dataset (*n* = 1,000,000, 100,000, and
292 1,000,000 for the Sinnamary, Amazon, and PSR coastal zones, respectively),
293 with Gelman diagnostic variables lower than 1.05. Isotopic fractionation factors
294 used for the models were calculated for each area and possible sources
295 (Supplementary Table 2). The prior was set as “uninformative”, where prior: α=
296 c(1,1,1).

297 Two-endmember (Equation 1) (Schultz and Calder, 1976) and three-
298 endmember linear models (Equation 2) (Fry, 2013) were used to evaluate the
299 contributions of common terrestrial sources (terrestrial C_3 plants) for each
300 sample to evaluate BC content associations:

301

302 Eq. 1: C_3 plants $= \left(\frac{\delta^{13}C_{Marine} - \delta^{13}C_{Sample}}{\delta^{13}C_{Marine} - \delta^{13}C_{Terrestrial}}\right) \bullet 100$

303

304 Where $\delta^{13}C_{Sample}$ is equivalent to the value found for a given sample, and
305 $\delta^{13}C_{Terrestrial}$ and $\delta^{13}C_{Marine}$ are the isotopic composition values for terrestrial and
306 marine sources, respectively. The assumed $\delta^{13}C$ value for the terrestrial C_3 plant
307 endmember was -31.8 ‰ (Martinelli et al., 2021) versus -19.9 ‰ for the marine
308 end-member (Bianchi et al., 2018) for the Amazon samples. As potential OM
309 sources for the Sinnamary and PSR coastal zones are different, the model
310 presenting the respective $\delta^{13}C$ and $\delta^{15}N$ values for each area was employed
311 through the following equation (2):

312

313 Eq. 2: C_3 plants $= \frac{(\delta^{15}N_C - \delta^{15}N_B)\bullet(\delta^{13}C_{Sample} - \delta^{13}C_B) - (\delta^{13}C_C - \delta^{13}C_B)\bullet(\delta^{15}N_{Sample} - \delta^{15}N_B)}{(\delta^{15}N_C - \delta^{15}N_B)\bullet(\delta^{13}C_A - \delta^{13}C_B) - (\delta^{13}C_C - \delta^{13}C_B)\bullet(\delta^{15}N_A - \delta^{15}N_B)}$

314

315 Where $\delta^{13}C_{Sample}$ and $\delta^{15}N_{Sample}$ comprise the isotopic composition values
316 of the sediment samples. For the Sinnamary coastal zone, A, B, and C represent
317 the OM sources originating from terrestrial C_3 plants (mangrove),
318 microphytobenthos (MPB), and marine phytoplankton, respectively. The $\delta^{13}C$ and
319 $\delta^{15}N$ values for the assessed mangrove (*Avicennia germinans* litter) were assumed
320 to be -30.1 and 2.6 ‰, respectively, versus -20.9 and 4.6 ‰ for MPB (Ray et al.,
321 2018). The marine source values during the wet season were -23.9 and 3.4 ‰ for
322 $\delta^{13}C$ and $\delta^{15}N$, respectively (Matos et al., 2020). Concerning the PSR coastal zone,
323 the isotopic compositions of A, B, and C represent terrestrial C_3 plant, marine
324 phytoplankton, and terrestrial C_4 plant sources, respectively. The $\delta^{13}C$ and $\delta^{15}N$

values for the terrestrial C_3 plant source were -31.3 and 2.7 ‰, respectively (Martinelli et al., 2021). Concerning marine phytoplankton, $\delta^{13}C$ and $\delta^{15}N$ values were -19.0 and 7.5 ‰, respectively (Gatts et al., 2020). The isotopic C and N values for terrestrial C_4 plants were -14.6 ‰ (Ribas, 2012) and 7.1 ‰ (*internal unpublished data*), respectively.

The endmembers used for Equations 1 and 2 were the same as those employed for the Bayesian Mixing model, chosen based on literature values for each area, as different environmental settings can affect source isotopic compositions, such as latitude and altitude. The use of CO_2 by phytoplankton likely differs between the Sinnamary and Amazon coastal areas, due to distance from the coast, which could affect the isotopic compositions of the OM sources. Therefore, marine contributions for the Sinnamary coastal sediments were also considered, due to mangrove proximity.

2.6. Burial Flux

The BC burial fluxes (F_{burial}) in coastal sediments were estimated through Equation (3) (Sánchez-García et al., 2013):

Eq. 3: $F_{burial} = BC \cdot DBD \cdot SAR \cdot (1 - \Phi)$

Where BC is the sum of B5CA and B6CA (μg g^{-1}), DBD is the dry bulk density (g cm^{-3}), and SAR is the sedimentation accumulation rate (cm yr^{-1}). The DBD values were calculated for each sample (Supplementary Table 3). SAR values were 0.74 (Allison and Lee, 2004) and 0.6 (Wanderley et al., 2013) for the Sinnamary and PSR coastal zones, respectively. The SAR values differed for the Amazon set sample (Supplementary Table 3), in agreement with Sobrinho et al.

(2021), who grouped four different Amazon continental shelf regions presenting different deposition rates and sediment structures. Thus, SAR values differed among samples according to proximity to regions I, II and III (Supplementary Table 1). The central porosity value (0.75) commonly applied for global calculations was applied (Jönsson et al., 2003) to the Amazon and PSR coastal zones, while 0.5 was applied to the Sinnamary coastal zone, according to Aschenbroich et al. (2016).

2.7. Statistical analyses

Statistical analyses were performed using the R software (R Core Team, 2018). Descriptive statistics comprising medians and interquartile ranges were employed. Differences in $\delta^{13}C$ (‰) values between the evaluated coastal zones were verified by the Kruskal Wallis test, while BC (mg g^{-1} TOC) and B6CA:B5CA contents were evaluated by an ANOVA test (*aov*, Base Package, R Core Team, 2018) followed by a multiple comparison test (*Tukey HSD*, base package, R Core Team, 2018) assuming a 95 % confidence level. Model assumptions (normality, linearity, and residual homoscedasticity) were tested by a maximum likelihood function (*boxcox*, MASS package, Venables and Ripley, 2002). If a transformation was indicated by the function, the correct adjustment was performed. The Pearson correlation analysis was performed to assess potential correlations between all analyzed parameters (distance from river mouths, $\delta^{13}C$, BC, contribution of terrestrial C_3 plant OM).

Furthermore, non-linear regression models were used to evaluate the associations and behaviors between $\delta^{13}C$, BC and the B6CA:B5CA ratios and river mouth distances (*lm*, Base Package, R Core Team, 2018). Additionally, a linear model was constructed to assess associations between BC and the

375 contribution of terrestrial C_3 plants to infer BC sources (*lm*, Base Package, R Core
376 Team, 2018). Model assumptions (normality, linearity, and residual
377 homoscedasticity) were tested using a maximum likelihood function (*boxcox*,
378 MASS package, Venables and Ripley, 2002); when a transformation was indicated
379 by the function, the correct adjustment was applied.

380 **3. RESULTS**

381 **3.1. Organic matter sources**

382 The $\delta^{13}C$ values from the coastal zone PSR OM were more ^{13}C-enriched
383 (-22.6 ± 1.3 ‰, Kruskal-Wallis test $p < 0.01$) compared to the Sinnamary and
384 Amazon River coastal sediments (-25.0 ± 3.1 and -26.1 ± 1.0 ‰, respectively)
385 (Figure 2A; Supplementary Table 2). The $\delta^{13}C$ OM values ranged between -27.7
386 and -25.1 ‰, -32.4 and -20.7 ‰, and -24.8 and -20.4 ‰ for the Sinnamary,
387 Amazon, and PSR coastal zones, respectively, with a trend towards ^{13}C
388 enrichment with increasing distances from the Amazon and PSR river mouths
389 (Figure 2B).

390

391 **Figure 2.** Boxplots for $\delta^{13}C$ OM values (n = 6, 14 and 13, for Sinnamary,
392 Amazon and PSR coastal zones, respectively) (A) and distribution according to
393 river mouth distance (log km) (B). Different letters represent statistical
394 significance for the difference in the means (Kruskal-Wallis tests, $p < 0.01$) and
395 the circles represent outliers (A). Red symbol values were not used in model
396 construction.

397

398 The contribution of potential OM sources to the investigated sediment
399 samples were determined by coupling $\delta^{13}C$ and $\delta^{15}N$ values (Figure 3A). Bayesian

400 stable isotope mixing models were used to determine OM sources (Figure 3B).
401 The estimated relative percentages of OM-contributing sources for Sinnamary
402 River coastal sediments averaged 36.7, 26.4, and 37.0 % for marine sources,
403 MPB, and terrestrial C_3 plants, respectively. Marine sources accounted for 48.7
404 % of the OM for Amazon coastal sediments, while terrestrial C_3 plants
405 presented a significant contribution of 51.3 %. Contributions for PSR coastal
406 sediments were 39.5 % marine, 35.6 % terrestrial C_3 plants, and 24.9 %
407 terrestrial C_4 plants.
408
409 **Figure 3.** Cross-plot of $\delta^{13}C$ *vs* $\delta^{15}N$ TOC and TN values. Polygons represent
410 source material and lines represent the discrimination uncertainty (A). Relative
411 contribution of the different sources for the investigated coastal zones (B). The
412 $\delta^{13}C$ source material values were obtained from Ometto et al. (2006), Hamilton and
413 Lewis (1992), Bouillon et al. (2011), Ray et al. (2018) and Ribas (2012). The $\delta^{15}N$
414 values were obtained from Ometto et al. (2006), Caraballo et al. (2014), Ray et al.
415 (2018), and Ribas (2012).
416
417 **3.2. Black carbon in coastal zones**
418 Black carbon normalized by TOC content differed between the Amazon
419 (0.32 ± 0.24 mg g^{-1} TOC) and PSR (0.95 ± 0.74 mg g^{-1} TOC) coastal zones
420 (one-way ANOVA: p = 0.035), both of which exhibited similar concentrations to
421 Sinnamary coastal sediments (0.73 ± 0.67 mg g^{-1} TOC; Figure 4A). In addition,
422 BC contents were moderately and positively correlated with TOC in the
423 Sinnamary and Amazon coastal sediments (r = 0.60 and 0.66, respectively;
424 Supplementary Figure 1) and moderately and negatively correlated with TOC in

PSR coastal sediments (r = -0.60; Supplementary Figure 1). Concerning the PSR coastal zone, BC contents generally increased with river mouth distance, while a strong drop in BC contents was noted for both the Amazon and Sinnamary coastal sediments, with BC initially increasing followed by a rapid drop associated to river mouth distance (Figure 4C). The B6CA:B5CA ratios, used to assess BC degree of condensation, were highest in the PSR coastal zone samples (one-way ANOVA: F = 4.826, p < 0.05) compared to the other investigated coastal zones (Figure 4B). The B6CA:B5CA ratios for the Sinnamary, Amazon, and PSR sediments were 0.28 ± 0.17, 0.29 ± 0.23, and 0.50 ± 0.15, respectively (Figure 4B). The trends of the B6CA:B5CA ratios were not significant (Figure 4D).

Figure 4. Boxplots for BC values normalized to TOC content (A) and B6CA:B5CA ratios (B) (n = 6, 8 and 13, for Sinnamary, Amazon and PSR coastal zones, respectively). Relationship between BC content (C) and B6CA:B5CA ratios (D) concerning distance from the Sinnamary, Amazon, and PSR River mouths (log km). Letters represent the statistical significances for the differences in mean values (Tukey's test, p < 0.05), and circles represent outliers (A). Red symbols indicate values that were not used in model construction.

Potential BC sources for the investigated coastal zones were inferred employing the relationship between C_3 plant contributions (Eq. 1 and 2) and sedimentary OM and BC contents (Figure 5). Black carbon contents increased with

449 increasing C_3 plant OM contributions for the Sinnamary and Amazon coastal
450 sediments, while the opposite was observed for the PSR.
451
452 **Figure 5.** Contribution of terrestrial C_3 plants to OM *vs* BC content in
453 Sinnamary, Amazon, and PSR coastal zone sediments. Data points with red
454 symbols were not used in model construction.
455 The estimated BC burial fluxes were 2.19 ± 2.23, 0.13 ± 0.13 and 2.39 ±
456 1.50 μg cm^2 yr^{-1} for the Sinnamary, Amazon, and PSR coastal zones,
457 respectively, with the lowest value observed for Amazon coastal zone.
458 **4. DISCUSSION**
459 **4.1. Organic matter coastal sediment sources reflect land-use changes**
460 The detected ^{13}C enrichment of the PSR coastal sediments represents
461 a typical signal of terrestrial C_3-C_4 plant mixtures, reflecting land-use changes in
462 the PSR drainage basin (Figure 2A). The enrichment of $\delta^{13}C$ values can be
463 observed after decades of land-cover changes, decreasing from -25.1 to -20.2
464 ‰ in 50 years, as described by Vitorello et al. (1989). Ribas (2012) analyzed
465 vegetation and soil $\delta^{13}C$ values in the PSR basin and reported that $\delta^{13}C$ soil and
466 vegetation samples differed by around 5 ‰. The same trend was observed in
467 forest areas, with more ^{13}C enriched soil values. As reported by Boschker and
468 Middelburg (2002), the difference between forest vegetation and forest soils can
469 be explained by the preferential use of ^{12}C compared to ^{13}C by microorganisms
470 during OM soil mineralization (Blagodatskaya et al., 2011; Liu and Han, 2021),
471 while different values for C_4 vegetation and soil can be explained by the land-
472 use change. Concerning the PSR fluvial system, Marques (2017) reported ^{13}C-
473 enriched values ranging from -25 to -23 ‰ for SPM, with C_4 plant contributions

474 ranging from 27 to 40 % to particulate organic carbon, even after centuries of
475 land-use change (Ribeiro et al., 2009). When reaching the aquatic system, the
476 particulate organic carbon (POC) receives autochthonous material, such as
477 from freshwater phytoplankton, with $\delta^{13}C$ values according to dissolved
478 inorganic carbon in the water column used for photosynthesis (Vuorio et al.,
479 2006). In the estuarine zone, POC $\delta^{13}C$ values observed by Marques (2017)
480 were more ^{13}C depleted, ranging from -25.8 to -23.7 ‰, indicating mangrove
481 contributions (terrestrial C_3 plants) that, in addition to autochthonous
482 contributions, can dilute terrestrial C_4 plant contributions to coastal sediments.
483 Indeed, according to the MixSIAR model, the terrestrial C_3 plant contribution to
484 TOC content was higher than that of terrestrial C_4 plants (Figure 3B), while
485 marine production was the primary source for PSR coastal sediments. The
486 marine source being so evident in the mixture of the MO can be attributed to
487 low river discharge during the sampling period, to low precipitation rates, which
488 were below 50 % of normally expected values due to a La Niña macroclimatic
489 event (Marques et al., 2017) and to anthropogenic PSR watershed
490 modifications (Carvalho et al., 2002; Souza et al., 2010).

491 Sedimentary OM in the Amazon and Sinnamary coastal zones exhibited
492 a strong C_3 plant signal, as expected, since local rainforests are dominated by
493 these types of plants (Figures 1 and 2A). Therefore, the ^{13}C enrichment noted
494 for Amazon coastal sediments highlights the increasing contribution of marine
495 OM sources with increasing river mouth distances (Figure 2B, Supplementary
496 Figure 1B). The determined sedimentary isotopic C and N composition indicates
497 that marine sources contributed considerably to several surface sediment
498 samples (Figure 3A), in line with previous studies demonstrating that offshore

499 TOC is mainly derived from marine primary production (Aller and Blair, 2006;
500 Sobrinho et al., 2021). Ward et al. (2015) reported that about 50 % of
501 continental OM does not reach the Amazon coastal zone due to intense OM
502 river remineralization and sedimentation. In addition, according to Sobrinho et
503 al. (2021), terrestrial OM that reaches the Amazon River delta comprises the
504 main OM sediment source. Organic matter is, however, continuously
505 remineralized in the Amazon River plume and terrestrial OM is replaced by
506 marine OM, which explains the strong ^{13}C enrichment noted with increasing
507 river mouth distances (Aller and Blair, 2006) (Figures 2B and 3B). This trend
508 has also been reported by Sun et al. (2017), who detected ^{13}C-enriched isotopic
509 values ranging from -21.4 and -23.0 ‰ in Amazon fan sediments. Additionally,
510 by analyzing lignin phenols, these authors also demonstrated that terrestrial OM
511 reaching the Amazon plume undergoes extensive diagenetic alterations before
512 being deposited, as previously suggested by Aller and Blair (2006) and Ward et
513 al. (2015).

514 Sinnamary coastal sediments exhibited a dominance of C_3 vegetation
515 (e.g*.,* from the extensive surrounding mangrove, river-transported debris, and
516 autochthonous production) (Figure 3). When investigating SPM at the
517 Sinnamary estuary, Ray et al. (2018) reported the same OM source as that
518 determined in the present study, also reporting significant contributions of the
519 MPB biofilm to coastal sediments. In addition, a major contribution of terrestrial
520 C_3 plants was noted by applying the equation model to determine the
521 contribution for each sample, except for the sample collected near the pioneer
522 mangrove area, where around 55 % of sediment OM originated from MPB.
523 Conversely, the surface sediment sample from the adult mangrove area

exhibited the lowest MPB contribution (14 %) and the highest terrestrial C_3 plant contribution (75 %). According to Marchand et al. (2003), the abundance of MPB biofilms decreases with increasing mangrove age due to decreased light availability caused by an increased canopy cover, hindering MPB photosynthesis. This ecological relationship explains the strong negative correlation observed herein between both sources (r = -0.89; Supplementary Figure 1A).

4.2. Land use BC drivers in coastal zones

Sedimentary BC contents differed between the investigated coastal zones, with the Amazon presenting lower values (Figure 4A). Indeed, no pyrogenic material was detected in six of the evaluated Amazon samples (Supplementary Table 1). The BPCA method includes the polycondensed aromatic BC fraction but does not detect labile pyrogenic molecules (Wagner et al., 2021) or the highly condensed fraction (Hammes et al., 2007). In addition, river mouth distance and river discharge likely play important roles in offshore BC transport. Less condensed pyrogenic material can be degraded in the fluvial portion of the land-ocean continuum, as turnover rates may range from days to weeks (Bird et al., 2015; Wagner et al., 2021). Therefore, the low BC content determined herein can be explained by dilution due to high river discharges. In addition, the high residence time of particles in river systems displaying extensive lowlands, such as the Amazon basin, can result in higher OM remineralization along the river system (Bianchi et al., 2018). Consequently, BC can be degraded and replaced by non-thermally modified OM in floodplains before reaching the coastal zone (Frueh and Lancaster, 2014; Cotrufo et al., 2016). This degradation in the river section of the land-ocean gradient may

549 explain the low BC content, while the source change of TOC content (terrestrial
550 to marine) explains the rapid BC content decline with increasing river mouth
551 distance (Figures 4A and C). The heterogeneity in the B6CA:B5CA ratios along
552 the land-ocean gradient indicates the presence of two mechanisms acting on
553 BC deposition in Amazon plume sediments, namely the removal of hydrophobic
554 components from the dissolved BC fraction by co-precipitation (Coppola et al.,
555 2014; Coppola et al., 2022), and the remobilization of aged BC from alluvial
556 sedimentary deposits (Wagner et al., 2018). The first mechanism has been
557 reported for the North Pacific Ocean, where dissolved BC contributes to
558 sediment BC content through the adsorption of highly condensed structures
559 (Nakane et al., 2017). This would explain why the sample with the highest BC
560 content was the one obtained at the greatest distance to the river mouth. The
561 second mechanism may be a consequence of energetic mixing and high
562 particle load of the Amazon River, where particles are subject to numerous
563 deposition and resuspension cycles during lateral transport. As a result, BC can
564 be stored in intermediate reservoirs before being stored in marine sediments
565 (McKee et al., 2004; Coppola et al., 2018).

566 Although the sedimentary BC contents at the Sinnamary River and PSR
567 coastal zones were comparable, different trends were observed with increasing
568 river mouth distances (Figures 4A and 4C). In contrast to BC transport along the
569 Amazon River land-ocean continuum, BC in small to medium-sized rivers such
570 as the Sinnamary and PSR reaches the coastal zone faster due to the relatively
571 short time between aquatic system entry and coastal sediment deposition
572 (Burdige, 2007). Black carbon content seems to be heterogenous in the
573 Sinnamary coastal zone, with a high BC contribution compared to TOC in two

574 samples collected near the adult mangrove channel and in the middle estuary,
575 where estuarine mixing takes place (Figure 4C). Mangroves display a high
576 allochthonous fluvial OM sediment retention capacity (Chew and Gallagher,
577 2018). Chew and Gallagher (2018) attributed the high BC to TOC ratio detected
578 in mangrove sediments to fluvial BC transport, as mangroves rarely burn.
579 Moreover, it is essential to highlight the importance of soot-derived BC canopy
580 trapping (Agawin and Duarte, 2002; Chew and Gallagher, 2018). In the
581 estuarine mixing zone, flocculation, and subsequent deposition facilitates the
582 accumulation of fine particles, resulting in the deposition of thermally and non-
583 thermally modified OM (Eisma et al., 1994). The removal of hydrophobic
584 structures from dissolved BC may also explain the increasing B6CA:B5CA
585 ratios of the sediment samples with increasing river mouth distance, also
586 observed in the Amazon coastal sediments. The increasing B6CA:B5CA ratios
587 with increasing distance from the Sinnamary river mouth can also be explained
588 by atmospheric soot deposition since soot contains the most aromatic form of
589 BC (Wolf et al., 2013; Saiz et al., 2015; Jones et al., 2017).
590 The BC content increased with increasing distance from the PSR mouth
591 (Figure 4C and Supplementary Figure 1C), and the evaluated sediments
592 exhibited higher BC condensation values (Figure 4B), highlighting the refractory
593 nature of BC in this coastal region. Saiz et al. (2015) observed a higher
594 production of stable and refractory material in landscapes consisting mainly of
595 grasses. The same trend observed by Wolf et al. (2013), with B6CA:B5CA
596 ratios for forest and grass produced from immediate natural fires being 0.63 ±
597 0.12 and 0.99 ± 0.27, respectively. Thus, the current BC production in the PSR
598 basin can explain the higher B6CA:B5CA ratios and the stability trend of

599 thermally-modified OM along the land-ocean gradient. By applying the
600 relationship between BC and the contribution of terrestrial C_4 plants, Marques et
601 al. (2017) identified historical Atlantic Rainforest burning as the predominant
602 source of dissolved BC in the PSR, as also suggested by Dittmar et al. (2012a),
603 with B6CA:B5CA ratios ranging between 0.27 and 0.38. As mentioned
604 previously, BC soil solubilization and its subsequent entry into the aquatic
605 system can take decades (Dittmar et al., 2012b). It is therefore expected that
606 BC originating from historical burning is mobilized from soils mainly by soil OM
607 solubilization (Dittmar et al., 2012a). Changes in vegetation cover and current
608 BC production increase soil erosion (Smith et al., 2011), making the input of
609 particles into the aquatic system more significant for recently produced BC.
610 When estimating BC content in SPM and dissolved OM, Wagner et al. (2015)
611 reported an immediate BC contribution to SPM, with a decrease following the
612 burning event, but increasing again during spring and late summer rain due to
613 higher runoff. However, land-use fire management in pasture and sugar-cane
614 areas takes place annually in the PSR basin (Ferreira et al., 2021), continuously
615 increasing the BC soil pool. Thus, the difference in BC sources and quality
616 between the sediment compartments in the present study and the dissolved
617 fraction in Marques et al. (2017) can be explained by differences in molecular
618 composition modulation for the dissolved and particulate water fractions
619 (Wagner et al., 2018).

620 **4.3. BC sources and burial fluxes in coastal zones**

621 The thermally modified OM in the sediment compartment of the
622 evaluated coastal zones varied with the current vegetation cover of each basin
623 (Figure 5). However, the estimated contribution of C_3 plants does not distinguish

624 vascular plants from autochthonous production in river waters, leading to a
625 “mixture” factor in the determination coefficient. Historical Atlantic Rainforest
626 burning explains the dissolved BC concentrations at the PSR (Marques et al.,
627 2017), although sedimentary BC contents decreased with increasing terrestrial
628 C_3 OM source contributions in PSR coastal sediments (Figure 5). A high BC
629 content (2.37 mg g^{-1} TOC) detected in one sample without contribution from
630 terrestrial C_4 plants with a low B6CA:B5CA ratios may indicate the presence of
631 old BC originating from historical Atlantic Rainforest burning or even from sugar
632 cane fields that have been fire-managed for centuries in this area (Marques et
633 al., 2017). Jones et al. (2017) highlighted the importance of atmospheric soot
634 deposition for BC content in the PSR, indicating that recently produced soot
635 (e.g., from biomass or fossil fuel burning) can be introduced into the water
636 column after atmospheric deposition, being subsequently transported along with
637 river SPM to be deposited in the coastal zone. Thus, in addition to riverine BC
638 transport, BC can also originate from atmospheric deposition (Lara et al., 2005).
639 In contrast, atmospheric transport to the Amazon and Sinnamary River mouths
640 appears to not be significant concerning sedimentary BC contents. According to
641 Coppola et al. (2019), BC originating from atmospheric deposition can be
642 rapidly removed or diluted in the fluvial sector of the Amazon River. In the PSR
643 coastal zone however, a constant BC supply to the coastal zone is directly
644 linked to the annual fire management of croplands and pasture areas.
645 Black carbon burial flux estimates for coastal zones are important to
646 better understand the role of thermally modified OM in the global carbon cycle,
647 as burial in coastal sediments is an essential BC sink (Sánchez-García et al.,
648 2013; Bird et al., 2015). The burial flux observed for the Amazon coastal zone

649 was significantly lower compared to the other investigated coastal zones (one-
650 way ANOVA: $p < 0.001$) and was strongly and negatively correlated with
651 increasing river mouth distance ($r = -0.88$). Similarly, no differences between the
652 Sinnamary and PSR coastal zones were observed. Including the B3CA and
653 B4CA markers increased the burial flux for PSR coastal to values between 2.61
654 and 306.19 µg cm^{-2} y^{-1}, which is, for example, lower than the burial flux reported
655 by Sánchez-García et al. (2013) in the Gulf of Cádiz, Spain. However, since
656 different BC determination methods along the combustion continuum are
657 available (e.g., including B3CA and B4CA in BC content estimates and/or
658 applying conversion factors [Glaser et al., 1998]), BC data derived from different
659 analytical techniques should be compared cautiously (Masiello, 2004;
660 Schneider et al., 2011; Kappenberg et al., 2016).

661 Black carbon contents can also be associated to organic and inorganic
662 pollutants (Nam et al., 2008; Liam and Xing, 2017). For example, Neupane et
663 al. (2020) reported a positive correlation between BC contents (mainly produced
664 by biomass burning) and Hg concentrations ($R^2 = 0.48$, $p < 0.001$), suggesting
665 similar sources and/or transport mechanisms in Selin Co lake surface
666 sediments, located in the central Tibetan Plateau. At the PSR coastal zone, the
667 constant BC input to the coastal zone is most likely directly associated to the
668 annual management of croplands and pasture areas (Ferreira et al., 2021) while
669 Hg is used in the sugar-cane management against pests (Câmara et al., 1986).
670 Therefore, Hg can be released to the atmosphere by soil volatilization during
671 the fire management of croplands and pasture areas and, alongside BC, is
672 transported to aquatic systems, either by fluvial or atmospheric transport.
673 Moreover, Nam et al. (2008) reported a correlation between BC and persistent

674 organic pollutants, although they emphasized that this relationship could be
675 masked by the old BC soil stocks. Consequently, understanding BC transport
676 and burial fluxes will aid in elucidating carbon sinks and also the fate of
677 contaminants in coastal sediments, especially considering that BC exhibits
678 environmental persistence.

679 **5. CONCLUSIONS**

680 In the present study, $\delta^{13}C$ coupled with $\delta^{15}N$ analyses and mixing
681 models were employed to understand the sources, composition, and spatial
682 dynamics of the organic matter in coastal sediments in northeastern South
683 American coastal zones in Brazil and French Guiana. Altered vegetation covers
684 from forests to grasslands were indicated as an OM modification driver in the
685 investigated coastal sediments. Additionally, we analyzed the contribution of
686 terrestrial OM (C_3 plants) to understand BC sources in the assessed drainage
687 basins. In PSR coastal sediments, a mixture of ^{13}C-enriched OM derived from
688 C_3 and C_4 plants, demonstrated that human-induced modifications from Atlantic
689 Rainforest to croplands and pasture areas altered the OM composition
690 transported to the coastal zone. Concerning the BC source for this drainage
691 basin, we suggest that BC produced from the incomplete burning of terrestrial
692 C_4 plant biomass is the main BC source for PSR coastal sediments (Figure 5;
693 Supplementary Figure 1), even though the $\delta^{13}C$ analysis was performed on bulk
694 TOC and not directly on molecular BC markers (BPCA).

695 Remineralization and sedimentation processes along the land-ocean
696 continuum of the Amazon River coupled to high river discharges can explain the
697 lower BC contents detected in the Amazon coastal zone compared to the PSR
698 and Sinnamary study sites. However, this could change in the future due to the

high agricultural expansion noted in the Amazon, which could exacerbate social and ecological impacts in this biome. Over the past 14 years, deforestation and forest fire rates in the Amazon have reached record levels, with anthropogenic activities increasingly removing Amazon Rainforest biomass, resulting in increased BC contents in soil and BC transported to the coastal zone. Even though land-use changes display the potential to produce more stable BC, it is crucial to consider that the Amazon rainforest accounts for 93 ± 23 Pg C stored aboveground, which can substantially increase BC production and lead to significant carbon cycle impacts.

Acknowledgments: Research in the French Guiana was co-funded by the French National Agency under the programs "Investissements d'Avenir" (LabexMER: ANR-10-LABX-19), by the CNRS MITI program (“Pépinière Interdisciplinaire de Guyane”) and by the French Research Institute for Sustainable Development (IRD). The International GEOTRACES Programme and support from the U.S. National Science Foundation (Grant OCE-1840868) to the Scientific Committee on Oceanic Research (SCOR) are also acknowledged. The German Science Foundation (DFG) is acknowledged for funding the *R/V* Meteor cruise M147. C.E. Rezende received financial support from CNPq (305217/2017-8) and FAPERJ (E-26/010.001272/2016 and E-26/200.893/2021), and this publication is part of his contribution to the INCT TMC*Ocean* on material transfer at the land-ocean interface. T. S. G. Serafim is grateful for the Master’s fellowship from CAPES as well to Heike Simon for all the support during the BPCA analysis at the Institute for Chemistry and Biology of the Marine Environment. This research is a GDR LIGA contribution.

6. REFERENCES

Agawin, N.S.R., Duarte, C.M., 2002. Evidence of direct particle trapping by a tropical seagrass meadow. Estuaries. https://doi.org/10.1007/bf02692217

Aller, R.C., 1998. Mobile deltaic and continental shelf muds as suboxic, fluidized bed reactors. Marine Chemistry. https://doi.org/10.1016/s0304-4203(98)00024-3

Aller, R.C., Blair, N.E., 2006. Carbon remineralization in the Amazon–Guianas tropical mobile mudbelt: A sedimentary incinerator. Continental Shelf Research. https://doi.org/10.1016/j.csr.2006.07.016

Aller, R.C., Blair, N.E., Xia, Q., Rude, P.D., 1996. Remineralization rates, recycling, and storage of carbon in Amazon shelf sediments. Continental Shelf Research. https://doi.org/10.1016/0278-4343(95)00046-1

Aller, R.C., Heilbrun, C., Panzeca, C., Zhu, Z., Baltzer, F., 2004. Coupling between sedimentary dynamics, early diagenetic processes, and biogeochemical cycling in the Amazon–Guianas mobile mud belt: coastal French Guiana. Marine Geology. https://doi.org/10.1016/j.margeo.2004.04.027

Allison, M.A., Lee, M.T., 2004. Sediment exchange between Amazon mudbanks and shore-fringing mangroves in French Guiana. Marine Geology. https://doi.org/10.1016/j.margeo.2004.04.026

Aragão, L.E.O.C., Anderson, L.O., Fonseca, M.G., Rosan, T.M., Vedovato, L.B., Wagner, F.H., Silva, C.V.J., Silva Junior, C.H.L., Arai, E., Aguiar, A.P., Barlow, J., Berenguer, E., Deeter, M.N., Domingues, L.G., Gatti, L., Gloor, M., Malhi, Y., Marengo, J.A., Miller, J.B., Phillips, O.L., Saatchi, S., 2018. 21st Century drought-related fires counteract the decline of Amazon deforestation carbon emissions. Nature Communication. https://doi.org/10.1038/s41467-017-02771-y

Aschenbroich, A., Michaud, E., Stieglitz, T., Fromard, F., Gardel, A., Tavares, M., & Thouzeau, G., 2016. Brachyuran crab community structure and associated sediment reworking activities in pioneer and young mangroves of French Guiana, South America. Estuarine Coastal and Shelf Science, 182, 60–71. https://doi.org/10.1016/j.ecss.2016.09.003

Bernardes, M.C., Martinelli, L.A., Krusche, A.V., Gudeman, J., Moreira, M., Victoria, R.L., Ometto, J.P.H., Ballester, M.V.R., Aufdenkampe, A.K., Richey, J.E., Hedges, J.I., 2004. Riverine organic matter composition as a function of land use change, Southwest Amazon. Ecological Applications. https://doi.org/10.1890/01-6028

Bernini, E., Rezende, C.E., 2004. Estrutura da vegetação em florestas de mangue do estuário do rio Paraíba do Sul, Estado do Rio de Janeiro, Brasil. Acta Botanica Brasilica. https://doi.org/10.1590/s0102-33062004000300009

Bianchi, T.S., Cui, X., Blair, N.E., Burdige, D.J., Eglinton, T.I., Galy, V., 2018. Centers of organic carbon burial and oxidation at the land-ocean interface. Organic Geochemistry. https://doi.org/10.1016/j.orggeochem.2017.09.008

Bird, M.I., Ascough, P.L., 2012. Isotopes in pyrogenic carbon: A review. Organic Geochemistry. https://doi.org/10.1016/j.orggeochem.2010.09.005

Bird, M.I., Wynn, J.G., Saiz, G., Wurster, C.M., McBeath, A., 2015. The Pyrogenic Carbon Cycle. Annual Review of Earth and Planetary Sciences. https://doi.org/10.1146/annurev-earth-060614-105038

Blagodatskaya, E., Yuyukina, T., Blagodatsky, S., Kuzyakov, Y., 2011. Turnover of soil organic matter and of microbial biomass under C3–C4 vegetation change: Consideration of 13C fractionation and preferential substrate utilization. Soil Biology and Biochemistry. https://doi.org/10.1016/j.soilbio.2010.09.028

Blair, N.E., Leithold, E.L., Ford, S.T., Peeler, K.A., Holmes, J.C., Perkey, D.W., 2003. The persistence of memory: the fate of ancient sedimentary organic carbon in a modern sedimentary system. Geochimica et Cosmochimica Acta. https://doi.org/10.1016/s0016-7037(02)01043-8

Boschker, H.T.S., Middelburg, J.J., 2002. Stable isotopes and biomarkers in microbial ecology. FEMS Microbiology Ecology. https://doi.org/10.1111/j.1574-6941.2002.tb00940.x

Bouillon, S., Connolly, R.M., Gillikin, D.P., 2011. Use of Stable Isotopes to Understand Food Webs and Ecosystem Functioning in Estuaries. Treatise on Estuarine and Coastal Science. https://doi.org/10.1016/b978-0-12-374711-2.00711-7

Brodowski, S., Rodionov, A., Haumaier, L., Glaser, B., Amelung, W., 2005. Revised black carbon assessment using benzene polycarboxylic acids. Organic Geochemistry. https://doi.org/10.1016/j.orggeochem.2005.03.011

Burdige, D.J., 2007. Preservation of Organic Matter in Marine Sediments: Controls, Mechanisms, and an Imbalance in Sediment Organic Carbon Budgets? ChemInform. https://doi.org/10.1002/chin.200720266

Cai, D.-L., Tan, F.C., Edmond, J.M., 1988. Sources and transport of particulate organic carbon in the Amazon River and estuary. Estuarine, Coastal and Shelf Science. https://doi.org/10.1016/0272-7714(88)90008-x

Câmara, V. de M., de M. Câmara, V., Campos, R.C., Perez, M.A., Tambelini, A.T., Klein, C.H., 1986. Teores de mercúrio no cabelo: um estudo comparativo em trabalhadores da lavoura de cana-de-açúcar com exposição pregressa aos fungicidas organo-mercuriais no município de Campos - RJ. Cadernos de Saúde Pública. https://doi.org/10.1590/s0102-311x1986000300008

Caraballo, P., Forsberg, B.R., de Almeida, F.F., Leite, R.G., 2014. Diel patterns of temperature, conductivity and dissolved oxygen in an Amazon

floodplain lake: description of a friagem phenomenon. Acta Limnologica Brasiliensia. https://doi.org/10.1590/s2179-975x2014000300011

Carvalho, C.E.V., Salomão, M.S.M., Molisani, M.M., Rezende, C.E., Lacerda, L.D., 2002. Contribution of a medium-sized tropical river to the particulate heavy-metal load for the South Atlantic Ocean. Science of The Total Environment. https://doi.org/10.1016/s0048-9697(01)00869-5

Chave, J., Riéra, B., Dubois, M.-A., 2001. Estimation of biomass in a neotropical forest of French Guiana: spatial and temporal variability. Journal of Tropical Ecology. https://doi.org/10.1017/s0266467401001055

Chew, S.T., Gallagher, J.B., 2018. Accounting for black carbon lowers estimates of blue carbon storage services. Sci. Rep. 8, 2553. https://doi.org/10.1038/s41598-018-20644-2

Cole, J.J., Prairie, Y.T., Caraco, N.F., McDowell, W.H., Tranvik, L.J., Striegl, R.G., Duarte, C.M., Kortelainen, P., Downing, J.A., Middelburg, J.J., Melack, J., 2007. Plumbing the Global Carbon Cycle: Integrating Inland Waters into the Terrestrial Carbon Budget. Ecosystems. https://doi.org/10.1007/s10021-006-9013-8

Coppola, A.I., Seidel, M., Ward, N.D., Viviroli, D., Nascimento, G.S., Haghipour, N., Revels, B.N., Abiven, S., Jones, M.W., Richey, J.E., Eglinton, T.I., Dittmar, T., Schmidt, M.W.I., 2019. Marked isotopic variability within and between the Amazon River and marine dissolved black carbon pools. Nature Communications. https://doi.org/10.1038/s41467-019-11543-9

Coppola, A.I., Wagner, S., Lennartz, S.T., Seidel, M., Ward, N.D., Dittmar, T., Santín, C., Jones, M.W., 2022. The black carbon cycle and its role in the Earth system. Nature Reviews Earth & Environment. https://doi.org/10.1038/s43017-022-00316-6

Coppola, A.I., Wiedemeier, D.B., Galy, V., Haghipour, N., Hanke, U.M., Nascimento, G.S., Usman, M., Blattmann, T.M., Reisser, M., Freymond, C.V., Zhao, M., Voss, B., Wacker, L., Schefuß, E., Peucker-Ehrenbrink, B., Abiven, S., Schmidt, M.W.I., Eglinton, T.I., 2018. Publisher Correction: Global-scale evidence for the refractory nature of riverine black carbon. Nature Geoscience. https://doi.org/10.1038/s41561-018-0252-z

Coppola, A.I., Ziolkowski, L.A., Masiello, C.A., Druffel, E.R.M., 2014. Aged black carbon in marine sediments and sinking particles. Geophysical Research Letters. https://doi.org/10.1002/2013gl059068

Cotrufo, M.F., Francesca Cotrufo, M., Boot, C.M., Kampf, S., Nelson, P.A., Brogan, D.J., Covino, T., Haddix, M.L., MacDonald, L.H., Rathburn, S., Ryan-Bukett, S., Schmeer, S., Hall, E., 2016. Redistribution of pyrogenic carbon from hillslopes to stream corridors following a large montane wildfire. Global Biogeochemical Cycles. https://doi.org/10.1002/2016gb005467

Dittmar, T., 2008. The molecular level determination of black carbon in marine dissolved organic matter. Organic Geochemistry. https://doi.org/10.1016/j.orggeochem.2008.01.015

Dittmar, T., de Rezende, C.E., Manecki, M., Niggemann, J., Ovalle, A.R.C., Stubbins, A., Bernardes, M.C., 2012a. Continuous flux of dissolved black carbon from a vanished tropical forest biome. Nature Geoscience. https://doi.org/10.1038/ngeo1541

Dittmar, T., Paeng, J., Gihring, T.M., Suryaputra, I.G.N., Huettel, M., 2012b. Discharge of dissolved black carbon from a fire-affected intertidal system. Limnology and Oceanography. https://doi.org/10.4319/lo.2012.57.4.1171

Edwards, P.J., 1984. The Use of Fire as a Management Tool. Ecological Studies. https://doi.org/10.1007/978-3-642-69805-7_16

Eisma, D., 1986. Flocculation and de-flocculation of suspended matter in estuaries. Netherlands Journal of Sea Research. https://doi.org/10.1016/0077-7579(86)90041-4

Eisma, D., Chen, S., Li, A., 1994. Tidal variations in suspended matter floc size in the Elbe river and Dollard estuaries. Netherlands Journal of Aquatic Ecology. https://doi.org/10.1007/bf02334194

Ferrante, L., Fearnside, P.M., 2019. Brazil's new president and "ruralists" threaten Amazonia's environment, traditional peoples and the global climate. Environmental Conservation. https://doi.org/10.1017/s0376892919000213

Ferreira, R., Nunes, C., Souza, M., Canela, M., 2021. Multivariate Optimization of Extraction Variables of PAH in Particulate Matter (PM10) in Indoor/Outdoor Air at Campos dos Goytacazes, Brazil. Journal of the Brazilian Chemical Society. https://doi.org/10.21577/0103-5053.20200216

Figueiredo, R. de O., de Oliveira Figueiredo, R., Ovalle, A.R.C., de Rezende, C.E., Martinelli, L.A., 2011. Carbon and Nitrogen in the Lower Basin of the Paraíba do Sul River, Southeastern Brazil: Element fluxes and biogeochemical processes. Ambiente e Agua - An Interdisciplinary Journal of Applied Science. https://doi.org/10.4136/ambi-agua.183

Forbes, M.S., Raison, R.J., Skjemstad, J.O., 2006. Formation, transformation and transport of black carbon (charcoal) in terrestrial and aquatic ecosystems. Sci. Total Environ. 370, 190–206. https://doi.org/10.1016/j.scitotenv.2006.06.007

Fromard, F., Vega, C., Proisy, C., 2004. Half a century of dynamic coastal change affecting mangrove shorelines of French Guiana. A case study based on remote sensing data analyses and field surveys. Marine Geology. https://doi.org/10.1016/j.margeo.2004.04.018

Frueh, W.T., Terry Frueh, W., Lancaster, S.T., 2014. Correction of deposit ages for inherited ages of charcoal: implications for sediment dynamics inferred from random sampling of deposits on headwater valley floors.

Quaternary Science Reviews. https://doi.org/10.1016/j.quascirev.2013.10.029
Fry, B., 2013. Alternative approaches for solving underdetermined isotope mixing problems. Marine Ecology Progress Series. https://doi.org/10.3354/meps10168
Gallo, M.N., Vinzon, S.B., 2015. Estudo numérico do escoamento em planícies de marés do canal Norte (estuário do rio Amazonas). Ribagua. https://doi.org/10.1016/j.riba.2015.04.002
Gatti, L.V., Basso, L.S., Miller, J.B., Gloor, M., Domingues, L.G., Cassol, H.L.G., Tejada, G., Aragão, L.E.O., Nobre, C., Peters, W., Marani, L., Arai, E., Sanches, A.H., Corrêa, S.M., Anderson, L., Von Randow, C., Correia, C.S.C., Crispim, S.P., Neves, R.A.L., 2021. Amazonia as a carbon source linked to deforestation and climate change. Nature. https://doi.org/10.1038/s41586-021-03629-6
Gatts, P.V., Franco, M.A.L., Almeida, M.G., Zalmon, I.R., Di Beneditto, A.P.M., Costa, P.A.S., de Rezende, C.E., 2020. The trophic ecology of marine catfishes in south-eastern Brazil. Journal of the Marine Biological Association of the United Kingdom. https://doi.org/10.1017/s0025315419001164
Geyer, W.R., Rockwell Geyer, W., Beardsley, R.C., Lentz, S.J., Candela, J., Limeburner, R., Johns, W.E., Castro, B.M., Soares, I.D., 1996. Physical oceanography of the Amazon shelf. Continental Shelf Research. https://doi.org/10.1016/0278-4343(95)00051-8
Glaser, B., Haumaier, L., Guggenberger, G., Zech, W., 1998. Black carbon in soils: the use of benzenecarboxylic acids as specific markers. Organic Geochemistry. https://doi.org/10.1016/s0146-6380(98)00194-6
Goldberg, E.D., 1985. Black Carbon in the Environment: Properties and Distribution. John Wiley and Sons, 1985.
Hamilton, S.K., Lewis, W.M., 1992. Stable carbon and nitrogen isotopes in algae and detritus from the Orinoco River floodplain, Venezuela. Geochimica et Cosmochimica Acta. https://doi.org/10.1016/0016-7037(92)90264-j
Hammes, K., Schmidt, M.W.I., Smernik, R.J., Currie, L.A., Ball, W.P., Nguyen, T.H., Louchouarn, P., Houel, S., Gustafsson, Ö., Elmquist, M., Cornelissen, G., Skjemstad, J.O., Masiello, C.A., Song, J., Peng, P. 'an, Mitra, S., Dunn, J.C., Hatcher, P.G., Hockaday, W.C., Smith, D.M., Hartkopf-Fröder, C., Böhmer, A., Lüer, B., Huebert, B.J., Amelung, W., Brodowski, S., Huang, L., Zhang, W., Gschwend, P.M., Xanat Flores-Cervantes, D., Largeau, C., Rouzaud, J.-N., Rumpel, C., Guggenberger, G., Kaiser, K., Rodionov, A., Gonzalez-Vila, F.J., Gonzalez-Perez, J.A., de la Rosa, J.M., Manning, D.A.C., López-Capél, E., Ding, L., 2007. Comparison of quantification methods to measure fire-derived (black/elemental) carbon in soils and sediments using

reference materials from soil, water, sediment and the atmosphere. Global Biogeochemical Cycles. https://doi.org/10.1029/2006gb002914
Hedges, J.I., Eglinton, G., Hatcher, P.G., Kirchman, D.L., Arnosti, C., Derenne, S., Evershed, R.P., Kögel-Knabner, I., de Leeuw, J.W., Littke, R., Michaelis, W., Rullkötter, J., 2000. The molecularly-uncharacterized component of nonliving organic matter in natural environments. Organic Geochemistry. https://doi.org/10.1016/s0146-6380(00)00096-6
Jones, M.W., Quine, T.A., de Rezende, C.E., Dittmar, T., Johnson, B., Manecki, M., Marques, J.S.J., de Aragão, L.E.O.C., 2017. Do Regional Aerosols Contribute to the Riverine Export of Dissolved Black Carbon? Journal of Geophysical Research: Biogeosciences. https://doi.org/10.1002/2017jg004126
Jönsson, A., Gustafsson, Ö., Axelman, J., Sundberg, H., 2003. Global Accounting of PCBs in the Continental Shelf Sediments. Environmental Science & Technology. https://doi.org/10.1021/es0201404
Jurado, E., Dachs, J., Duarte, C.M., Simó, R., 2008. Atmospheric deposition of organic and black carbon to the global oceans. Atmospheric Environment. https://doi.org/10.1016/j.atmosenv.2008.07.029
Kappenberg, A., Bläsing, M., Lehndorff, E., Amelung, W., 2016. Black carbon assessment using benzene polycarboxylic acids: Limitations for organic-rich matrices. Organic Geochemistry. https://doi.org/10.1016/j.orggeochem.2016.01.009
Kuehl, S.A., DeMaster, D.J., Nittrouer, C.A., 1986. Nature of sediment accumulation on the Amazon continental shelf. Continental Shelf Research. https://doi.org/10.1016/0278-4343(86)90061-0
Kuhlbusch, T.A.J., Crutzen, P.J., 1995. Toward a global estimate of black carbon in residues of vegetation fires representing a sink of atmospheric CO2 and a source of O2. Global Biogeochemical Cycles. https://doi.org/10.1029/95gb02742
Lara, L., Artaxo, P., Martinelli, L., Camargo, P., Victoria, R., Ferraz, E., 2005. Properties of aerosols from sugar-cane burning emissions in Southeastern Brazil. Atmospheric Environment. https://doi.org/10.1016/j.atmosenv.2005.04.026
Latrubesse, E.M., 2008. Patterns of anabranching channels: The ultimate end-member adjustment of mega rivers. Geomorphology. https://doi.org/10.1016/j.geomorph.2008.05.035
Laurance, W.F., Albernaz, A.K.M., Da Costa, C., 2001. Is deforestation accelerating in the Brazilian Amazon? Environmental Conservation. https://doi.org/10.1017/s0376892901000339
Lian, F., Xing, B., 2017. Black Carbon (Biochar) In Water/Soil Environments: Molecular Structure, Sorption, Stability, and Potential Risk. Environmental Science & Technology. https://doi.org/10.1021/acs.est.7b02528

Liu, J., Han, G., 2021. Tracing Riverine Particulate Black Carbon Sources in Xijiang River Basin: Insight from Stable Isotopic Composition and Bayesian Mixing Model. Water Research. https://doi.org/10.1016/j.watres.2021.116932

Lohmann, R., Bollinger, K., Cantwell, M., Feichter, J., Fischer-Bruns, I., Zabel, M., 2009. Fluxes of soot black carbon to South Atlantic sediments. Global Biogeochemical Cycles. https://doi.org/10.1029/2008gb003253

Major, J., Lehmann, J., Rondon, M., Goodale, C., 2010. Fate of soil-applied black carbon: downward migration, leaching and soil respiration. Global Change Biology. https://doi.org/10.1111/j.1365-2486.2009.02044.x

Malhi, Y., Roberts, J.T., Betts, R.A., Killeen, T.J., Li, W., Nobre, C.A., 2008. Climate change, deforestation, and the fate of the Amazon. Science 319, 169–172. https://doi.org/10.1126/science.1146961

Malhi, Y., Wood, D., Baker, T.R., Wright, J., Phillips, O.L., Cochrane, T., Meir, P., Chave, J., Almeida, S., Arroyo, L., Higuchi, N., Killeen, T.J., Laurance, S.G., Laurance, W.F., Lewis, S.L., Monteagudo, A., Neill, D.A., Vargas, P.N., Pitman, N.C.A., Quesada, C.A., Salomão, R., Silva, J.N.M., Lezama, A.T., Terborgh, J., Martínez, R.V., Vinceti, B., 2006. The regional variation of aboveground live biomass in old-growth Amazonian forests. Global Change Biology. https://doi.org/10.1111/j.1365-2486.2006.01120.x

Marchand, C., 2017. Soil carbon stocks and burial rates along a mangrove forest chronosequence (French Guiana). Forest Ecology and Management. https://doi.org/10.1016/j.foreco.2016.10.030

Marchand, C., Lallier-Vergès, E., Baltzer, F., 2003. The composition of sedimentary organic matter in relation to the dynamic features of a mangrove-fringed coast in French Guiana. Estuarine, Coastal and Shelf Science. https://doi.org/10.1016/s0272-7714(02)00134-8

Marques, J.S.J. (2017). Carbono negro dissolvido no contínuo continente-oceano no rio Paraíba do Sul (Doctoral dissertation, Tese de doutorado, Universidade Estadual do Norte Fluminense, 2017).

Marques, J.S.J., Dittmar, T., Niggemann, J., Almeida, M.G., Gomez-Saez, G.V., Rezende, C.E., 2017. Dissolved Black Carbon in the Headwaters-to-Ocean Continuum of Paraíba Do Sul River, Brazil. Frontiers in Earth Science. https://doi.org/10.3389/feart.2017.00011

Martinelli, L.A., Nardoto, G.B., Soltangheisi, A., Reis, C.R.G., Abdalla-Filho, A.L., Camargo, P.B., Domingues, T.F., Faria, D., Figueira, A.M., Gomes, T.F., Lins, S.R.M., Mardegan, S.F., Mariano, E., Miatto, R.C., Moraes, R., Moreira, M.Z., Oliveira, R.S., Ometto, J.P.H., Santos, F.L.S., Sena-Souza, J., Silva, D.M.L., Silva, J.C.S., Vieira, S.A., 2021. Determining ecosystem functioning in Brazilian biomes through foliar carbon and nitrogen concentrations and stable isotope ratios. Biogeochemistry. https://doi.org/10.1007/s10533-020-00714-2

Masiello, C.A., 2004. New directions in black carbon organic geochemistry. Marine Chemistry. https://doi.org/10.1016/j.marchem.2004.06.043

Matos, C.R.L., Berrêdo, J.F., Machado, W., Sanders, C.J., Metzger, E., Cohen, M.C.L., 2020. Carbon and nutrient accumulation in tropical mangrove creeks, Amazon region. Marine Geology. https://doi.org/10.1016/j.margeo.2020.106317

McKee, B.A., Aller, R.C., Allison, M.A., Bianchi, T.S., Kineke, G.C., 2004. Transport and transformation of dissolved and particulate materials on continental margins influenced by major rivers: benthic boundary layer and seabed processes. Continental Shelf Research. https://doi.org/10.1016/j.csr.2004.02.009

Nakane, M., Ajioka, T., Yamashita, Y., 2017. Distribution and Sources of Dissolved Black Carbon in Surface Waters of the Chukchi Sea, Bering Sea, and the North Pacific Ocean. Frontiers in Earth Science. https://doi.org/10.3389/feart.2017.00034

Nam, J.J., Gustafsson, O., Kurt-Karakus, P., Breivik, K., Steinnes, E., Jones, K.C., 2008. Relationships between organic matter, black carbon and persistent organic pollutants in European background soils: Implications for sources and environmental fate. Environmental Pollution. https://doi.org/10.1016/j.envpol.2008.05.027

Neupane, B., Wang, J., Kang, S., Zhang, Y., Chen, P., Rai, M., Guo, J., Yu, S., Thapa, P., 2020. Black carbon and mercury in the surface sediments of Selin Co, central Tibetan Plateau: Covariation with total carbon. Science of The Total Environment. https://doi.org/10.1016/j.scitotenv.2020.137752

Nittrouer, C.A., Curtin, T.B., DeMaster, D.J., 1986. Concentration and flux of suspended sediment on the Amazon continental shelf. Continental Shelf Research. https://doi.org/10.1016/0278-4343(86)90058-0

Oliveira, C. J., & Clavier, J., 2000. Space-time variations of suspended material in the Sinnamary estuary, French Guiana: influence of Petit Saut electric dam. Revista Brasileira de Oceanografia. https://doi.org/10.1590/S1413-77392000000100003

Ometto, J.P.H.B., Ometto, J.P.H., Ehleringer, J.R., Domingues, T.F., Berry, J.A., Ishida, F.Y., Mazzi, E., Higuchi, N., Flanagan, L.B., Nardoto, G.B., Martinelli, L.A., n.d. The stable carbon and nitrogen isotopic composition of vegetation in tropical forests of the Amazon Basin, Brazil. Nitrogen Cycling in the Americas: Natural and Anthropogenic Influences and Controls. https://doi.org/10.1007/978-1-4020-5517-1_12

Ovalle, A.R.C., Silva, C.F., Rezende, C.E., Gatts, C.E.N., Suzuki, M.S., Figueiredo, R.O., 2013. Long-term trends in hydrochemistry in the Paraíba do Sul River, south-eastern Brazil. Journal of Hydrology. https://doi.org/10.1016/j.jhydrol.2012.12.036

Parnell, A.C., Inger, R., Bearhop, S., Jackson, A.L., 2010. Source partitioning using stable isotopes: coping with too much variation. PLoS One 5, e9672. https://doi.org/10.1371/journal.pone.0009672

Ray, R., Michaud, E., Aller, R.C., Vantrepotte, V., Gleixner, G., Walcker, R., Devesa, J., Le Goff, M., Morvan, S., Thouzeau, G., 2018. The sources and distribution of carbon (DOC, POC, DIC) in a mangrove dominated estuary (French Guiana, South America). Biogeochemistry. https://doi.org/10.1007/s10533-018-0447-9

RC Team. (2018). R Foundation for Statistical Computing, Vienna, Austria, 2018. R: A language and environment for statistical computing.

Regnier, P., Friedlingstein, P., Ciais, P., Mackenzie, F.T., Gruber, N., Janssens, I.A., Laruelle, G.G., Lauerwald, R., Luyssaert, S., Andersson, A.J., Arndt, S., Arnosti, C., Borges, A.V., Dale, A.W., Gallego-Sala, A., Goddéris, Y., Goossens, N., Hartmann, J., Heinze, C., Ilyina, T., Joos, F., LaRowe, D.E., Leifeld, J., Meysman, F.J.R., Munhoven, G., Raymond, P.A., Spahni, R., Suntharalingam, P., Thullner, M., 2013. Anthropogenic perturbation of the carbon fluxes from land to ocean. Nature Geoscience. https://doi.org/10.1038/ngeo1830

Reisser, M., Purves, R.S., Schmidt, M.W.I., Abiven, S., 2016. Pyrogenic Carbon in Soils: A Literature-Based Inventory and a Global Estimation of Its Content in Soil Organic Carbon and Stocks. Frontiers in Earth Science. https://doi.org/10.3389/feart.2016.00080

Rezende, C.L., Scarano, F.R., Assad, E.D., Joly, C.A., Metzger, J.P., Strassburg, B.B.N., Tabarelli, M., Fonseca, G.A., Mittermeier, R.A., 2018. From hotspot to hopespot: An opportunity for the Brazilian Atlantic Forest. Perspectives in Ecology and Conservation. https://doi.org/10.1016/j.pecon.2018.10.002

Ribas, L. M. (2012). Caracterização de fontes de matéria orgânica do estuário do rio Paraíba do Sul, RJ, Brasil (Doctoral dissertation, Tese de doutorado, Universidade Estadual do Norte Fluminense, 2012. Tese 131p).

Ribeiro, M.C., Metzger, J.P., Martensen, A.C., Ponzoni, F.J., Hirota, M.M., 2009. The Brazilian Atlantic Forest: How much is left, and how is the remaining forest distributed? Implications for conservation. Biological Conservation. https://doi.org/10.1016/j.biocon.2009.02.021

Richard, S., Arnoux, A., Cerdan, P., Reynouard, C., & Horeau, V., 2000. Mercury levels of soils, sediments and fish in French Guiana, South America. Water, Air, and Soil Pollution, 124(3), 221-244. https://doi.org/10.1023/A:1005251016314

Richey, J.E., Meade, R.H., Salati, E., Devol, A.H., Nordin, C.F., Dos Santos, U., 1986. Water Discharge and Suspended Sediment Concentrations in the Amazon River: 1982-1984. Water Resources Research. https://doi.org/10.1029/wr022i005p00756

Rodionov, A., Amelung, W., Peinemann, N., Haumaier, L., Zhang, X., Kleber, M., Glaser, B., Urusevskaya, I., Zech, W., 2010. Black carbon in grassland ecosystems of the world. Global Biogeochemical Cycles. https://doi.org/10.1029/2009gb003669

Saiz, G., Wynn, J.G., Wurster, C.M., Goodrick, I., Nelson, P.N., Bird, M.I., 2015. Pyrogenic carbon from tropical savanna burning: production and stable isotope composition. Biogeosciences. https://doi.org/10.5194/bg-12-1849-2015

Sánchez-García, L., de Andrés, J.R., Gélinas, Y., Schmidt, M.W.I., Louchouarn, P., 2013. Different pools of black carbon in sediments from the Gulf of Cádiz (SW Spain): Method comparison and spatial distribution. Marine Chemistry. https://doi.org/10.1016/j.marchem.2013.02.006

Schneider, M.P.W., Smittenberg, R.H., Dittmar, T., Schmidt, M.W.I., 2011. Comparison of gas with liquid chromatography for the determination of benzenepolycarboxylic acids as molecular tracers of black carbon. Organic Geochemistry. https://doi.org/10.1016/j.orggeochem.2011.01.003

Shultz, D.J., Calder, J.A., 1976. Organic carbon variations in estuarine sediments. Geochimica et Cosmochimica Acta. https://doi.org/10.1016/0016-7037(76)90002-8

Silva, M.A.L., Calasans, C.F., Ovalle, A.R.C., Rezende, C.E., 2001. Dissolved Nitrogen and Phosphorus Dynamics in the Lower Portion of the Paraiba do Sul River, Campos dos Goytacazes, RJ, Brazil. Brazilian Archives of Biology and Technology. https://doi.org/10.1590/s1516-89132001000400006

Singh, N., Abiven, S., Torn, M.S., Schmidt, M.W.I., 2012. Fire-derived organic carbon in soil turns over on a centennial scale. Biogeosciences. https://doi.org/10.5194/bg-9-2847-2012

Smith, H.G., Sheridan, G.J., Lane, P.N.J., Nyman, P., Haydon, S., 2011. Wildfire effects on water quality in forest catchments: A review with implications for water supply. Journal of Hydrology. https://doi.org/10.1016/j.jhydrol.2010.10.043

Sobrinho, R. de L., de L. Sobrinho, R., Bernardes, M.C., de Rezende, C.E., Kim, J.-H., Schouten, S., Sinninghe Damsté, J.S., 2021. A multiproxy approach to characterize the sedimentation of organic carbon in the Amazon continental shelf. Marine Chemistry. https://doi.org/10.1016/j.marchem.2021.103961

Solórzano, A., de Assis Brasil, L.S.C., de Oliveira, R.R., 2021. The Atlantic Forest Ecological History: From Pre-colonial Times to the Anthropocene. The Atlantic Forest. https://doi.org/10.1007/978-3-030-55322-7_2

Souza, T.A., Godoy, J.M., Godoy, M.L.D., Moreira, I., Carvalho, Z.L., Salomão, M.S.M., Rezende, C.E., 2010. Use of multitracers for the study of water

mixing in the Paraíba do Sul River estuary. Journal of Environmental Radioactivity. https://doi.org/10.1016/j.jenvrad.2009.11.001

Stahl, C., Freycon, V., Fontaine, S., Dezécache, C., Ponchant, L., Picon-Cochard, C., Klumpp, K., Soussana, J.-F., Blanfort, V., 2016. Soil carbon stocks after conversion of Amazonian tropical forest to grazed pasture: importance of de.ep soil layers. Regional Environmental Change. https://doi.org/10.1007/s10113-016-0936-0

Stock B.C. and Semmens B.X., 2016. MixSIAR GUI User Manual. Version 3.1. https://doi:10.5281/zenodo.1209993

Stock, B.C., Jackson, A.L., Ward, E.J., Parnell, A.C., Phillips, D.L., Semmens, B.X., 2018 Analyzing mixing systems using a new generation of Bayesian tracer mixing models. https://doi.org/10.7287/peerj.preprints.26884v1

Stubbins, A., Spencer, R.G.M., Mann, P.J., Max Holmes, R., McClelland, J.W., Niggemann, J., Dittmar, T., 2015. Utilizing colored dissolved organic matter to derive dissolved black carbon export by arctic rivers. Frontiers in Earth Science. https://doi.org/10.3389/feart.2015.00063

Sun, S., Schefuß, E., Mulitza, S., Chiessi, C.M., Sawakuchi, A.O., Zabel, M., Baker, P.A., Hefter, J., Mollenhauer, G., 2017. Origin and processing of terrestrial organic carbon in the Amazon system: lignin phenols in river, shelf, and fan sediments. Biogeosciences. https://doi.org/10.5194/bg-14-2495-2017

Venables, W.N., Ripley, B.D., 2002. Modern Applied Statistics with S. Statistics and Computing. https://doi.org/10.1007/978-0-387-21706-2

Vitorello, V.A., Cerri, C.C., Andreux, F., Feller, C., Victória, R.L., 1989. Organic Matter and Natural Carbon-^{13} Distribution in Forested and Cultivated Oxisols. Soil Science Society of America Journal. https://doi.org/10.2136/sssaj1989.03615995005300030024x

Vuorio, K., Meili, M., Sarvala, J., 2006. Taxon-specific variation in the stable isotopic signatures (δ^{13}C and δ^{15}N) of lake phytoplankton. Freshwater Biology. https://doi.org/10.1111/j.1365-2427.2006.01529.x

Wagner, S., Cawley, K.M., Rosario-Ortiz, F.L., Jaffé, R., 2015. In-stream sources and links between particulate and dissolved black carbon following a wildfire. Biogeochemistry. https://doi.org/10.1007/s10533-015-0088-1

Wagner, S., Coppola, A.I., Stubbins, A., Dittmar, T., Niggemann, J., Drake, T.W., Seidel, M., Spencer, R.G.M., Bao, H., 2021. Questions remain about the biolability of dissolved black carbon along the combustion continuum. Nature Communications. https://doi.org/10.1038/s41467-021-24477-y

Wagner, S., Jaffé, R., Stubbins, A., 2018. Dissolved black carbon in aquatic ecosystems. Limnology and Oceanography Letters. https://doi.org/10.1002/lol2.10076

Wanderley, C.V.A., Godoy, J.M., Godoy, M.L.D., Rezende, C.E., Lacerda, L.D., Moreira, I., Carvalho, Z.L., 2013. Evaluating Sedimentation Rates in the Estuary and Shelf Region of the Paraíba do Sul River, Southeastern Brazil. Journal of the Brazilian Chemical Society. https://doi.org/10.5935/0103-5053.20130268

Ward, N.D., Krusche, A.V., Sawakuchi, H.O., Brito, D.C., Cunha, A.C., Moura, J.M.S., da Silva, R., Yager, P.L., Keil, R.G., Richey, J.E., 2015. The compositional evolution of dissolved and particulate organic matter along the lower Amazon River—Óbidos to the ocean. Marine Chemistry. https://doi.org/10.1016/j.marchem.2015.06.013

Wells, J.T., Coleman, J.M., 1981. Periodic mudflat progradation, northeastern coast of South America; a hypothesis. Journal of Sedimentary Research. https://doi.org/10.2110/jsr.51.1069

Werf, G.R. van der, van der Werf, G.R., Randerson, J.T., Giglio, L., van Leeuwen, T.T., Chen, Y., Rogers, B.M., Mu, M., van Marle, M.J.E., Morton, D.C., James Collatz, G., Yokelson, R.J., Kasibhatla, P.S., 2017. Global fire emissions estimates during 1997–2016. Earth System Science Data. https://doi.org/10.5194/essd-9-697-2017

Wilkinson, B.H., McElroy, B.J., 2007. The impact of humans on continental erosion and sedimentation. Geological Society of America Bulletin. https://doi.org/10.1130/b25899

Wolf, M., Lehndorff, E., Wiesenberg, G.L.B., Stockhausen, M., Schwark, L., Amelung, W., 2013. Towards reconstruction of past fire regimes from geochemical analysis of charcoal. Organic Geochemistry. https://doi.org/10.1016/j.orggeochem.2012.11.002

1223 FIGURES

1224

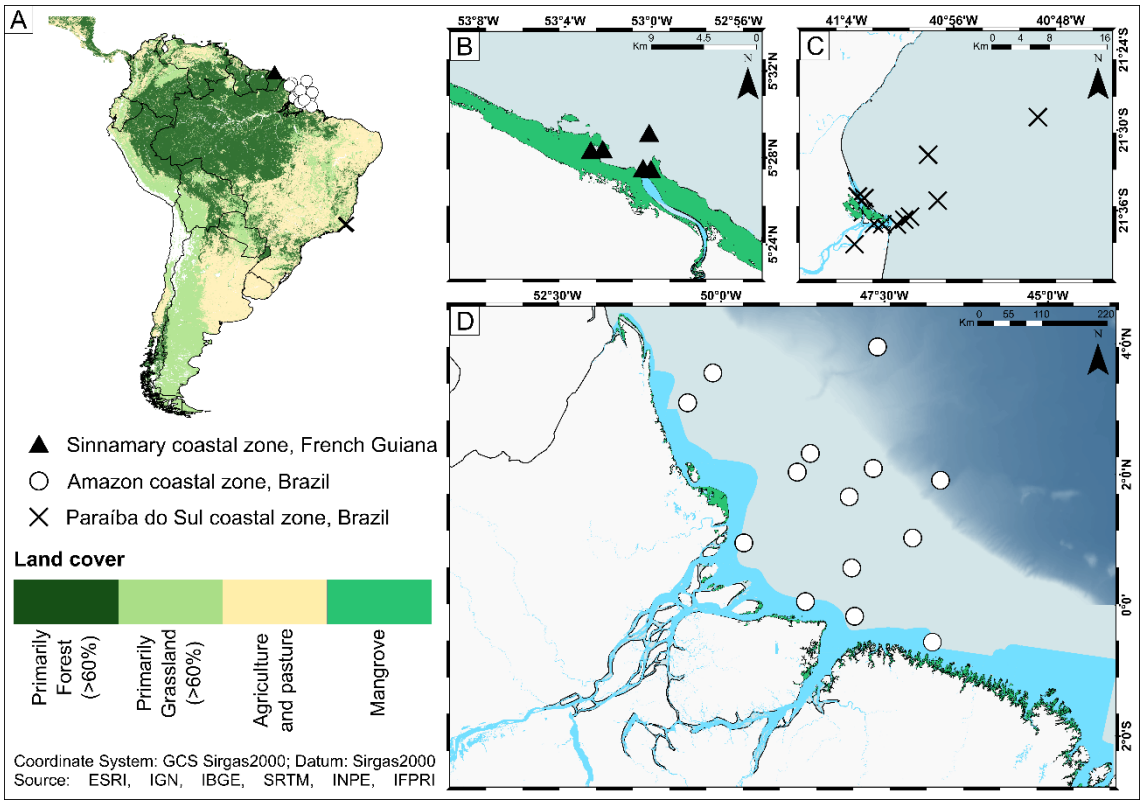

1225

1226 **Figure 6.** South America sediment sampling sites: (A) the Sinnamary estuary,
1227 in the French Guiana (B), the Paraíba do Sul River estuary, in southeastern
1228 Brazil (C) and the Amazon plume, in northern Brazil (D).

1229

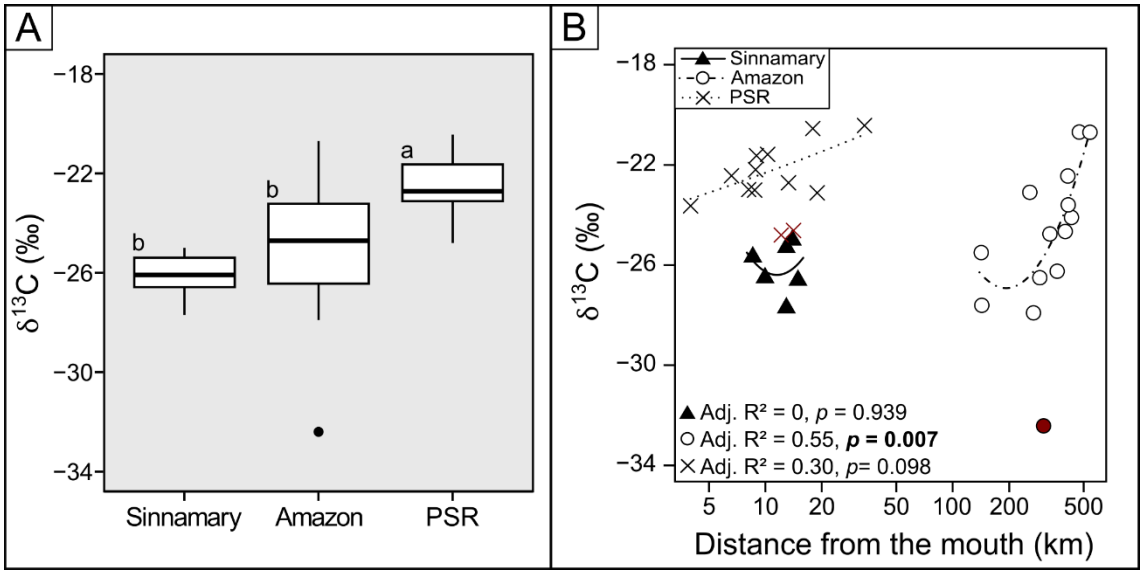

Figure 7. Boxplots for δ13C OM values (n = 6, 14 and 13, for Sinnamary, Amazon and PSR coastal zones, respectively) (A) and distribution according to river mouth distance (log km) (B). Different letters represent statistical significance for the difference in the means (Kruskal-Wallis tests, $p < 0.01$) and the circles represent outliers (A). Red symbol values were not used in model construction. (For interpretation of the references to color in this figure legend, the reader is referred to the web version of this article.)

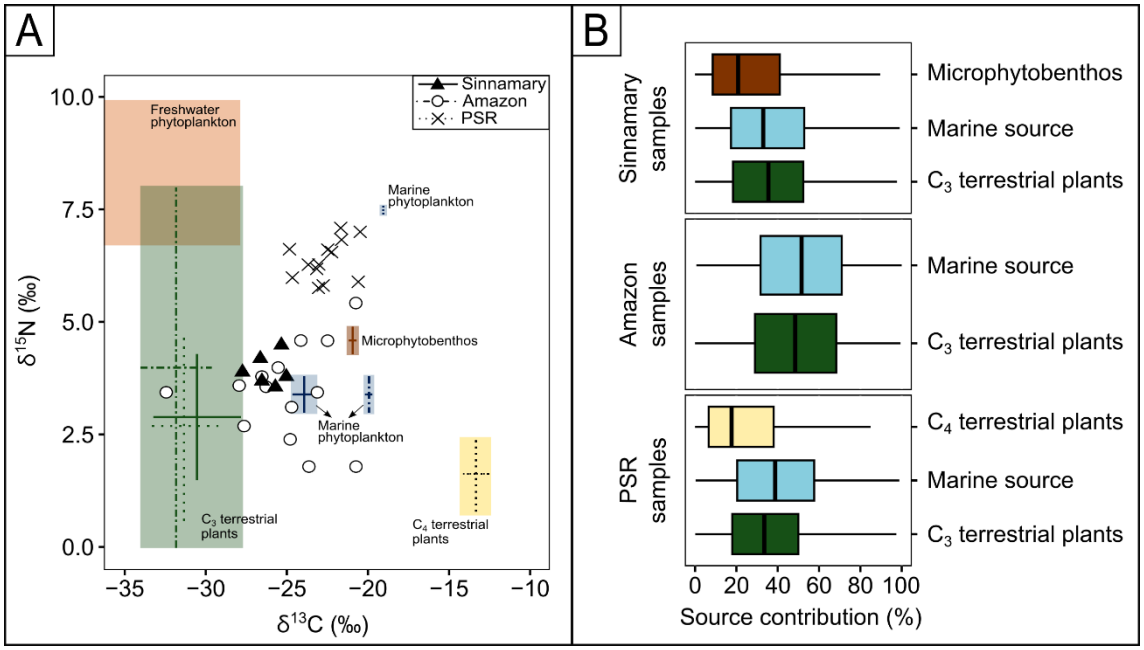

Figure 8. Cross-plot of δ13C vs δ15N TOC and TN values. Polygons represent source material and lines represent the discrimination uncertainty (A). Relative contribution of the different sources for the investigated coastal zones (B). The δ13C source material values were obtained from Ometto et al. (2006), Hamilton and Lewis (1992), Bouillon et al. (2011), Ray et al. (2018) and Ribas (2012). The δ15N values were obtained from Ometto et al. (2006), Caraballo et al. (2014), Ray et al. (2018), and Ribas (2012).

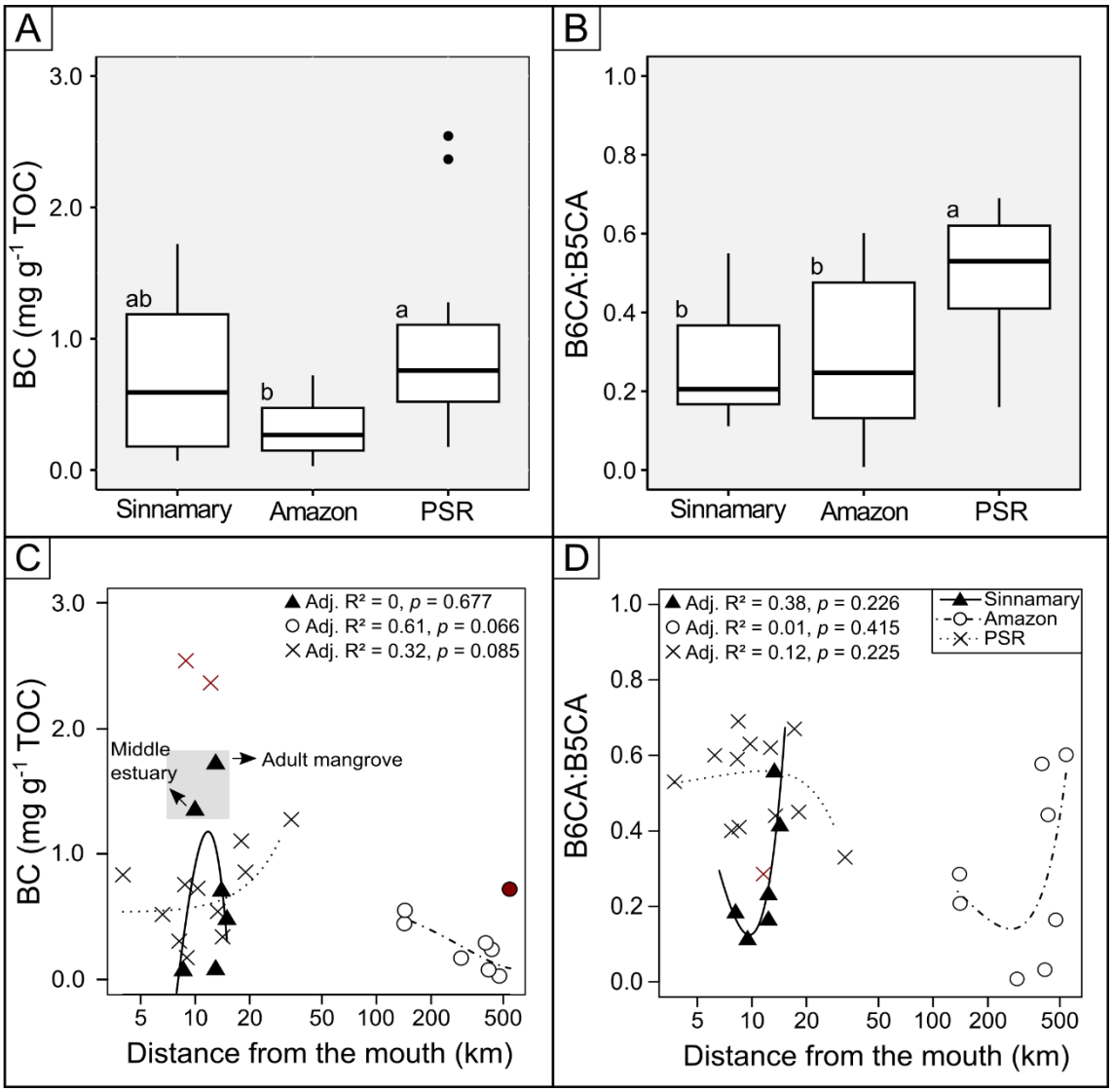

Figure 9. Boxplots for BC values normalized to TOC content (A) and B6CA:B5CA ratios (B) (n = 6, 8 and 13, for Sinnamary, Amazon and PSR coastal zones, respectively). Relationship between BC content (C) and B6CA:B5CA ratios (D) concerning distance from the Sinnamary, Amazon, and PSR River mouths (log km). Letters represent the statistical significances for the differences in mean values (Tukey's test, $p < 0.05$), and circles represent outliers (A). Red symbols indicate values that were not used in model construction. (For interpretation of the references to color in this figure legend, the reader is referred to the web version of this article.)

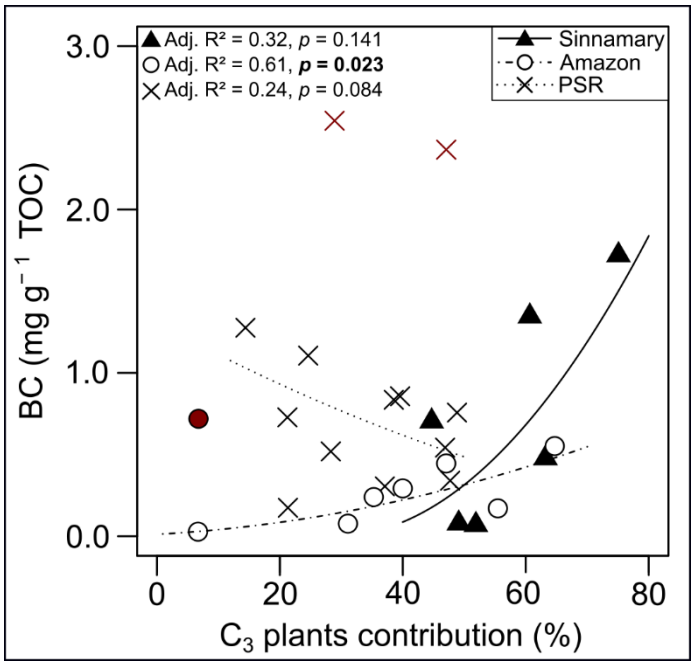

Figure 10. Contribution of terrestrial C3 plants to OM vs BC content in Sinnamary, Amazon, and PSR coastal zone sediments. Data points with red symbols were not used in model construction.